ADVANCES IN ATMOSPHERIC SCIENCES, VOL. 34, AUGUST 2017, 1017–1026

• **Original Paper** •

Optical Properties and Source Analysis of Aerosols over a Desert Area in Dunhuang, Northwest China

Yongjing MA[1,2], Jinyuan XIN[*2,3], Yining MA[1,2], Lingbin KONG[1,2], Kequan ZHANG[1], Wenyu ZHANG[1], Yuesi WANG[2], Xiuqin WANG[4], and Yongfeng ZHU[4]

[1]*College of Atmospheric Sciences, Key Laboratory of Arid Climatic Change and Reducing Disaster of Gansu Province, Lanzhou University, Lanzhou* 730000*, China*

[2]*State Key Laboratory of Atmospheric Boundary Layer Physics and Atmospheric Chemistry, Institute of Atmospheric Physics, Chinese Academy of Sciences, Beijing* 100029*, China*

[3]*College of Atmospheric Sciences, Chengdu University of Information Technology, Plateau Atmosphere and Environment Key Laboratory of Sichuan Province, Chengdu* 610225*, China*

[4]*Dunhuang Meteorological Bureau, Dunhuang* 736200*, China*

(Received 27 August 2016; revised 31 October 2016; accepted 29 November 2016)

ABSTRACT

Aerosol observational data for 2012 obtained from Dunhuang Station of CARE-China (Campaign on Atmospheric Aerosol Research Network of China) were analyzed to achieve in-depth knowledge of aerosol optical properties over Dunhuang region. The results showed that the annual average aerosol optical depth (AOD) at 500 nm was 0.32 ± 0.06, and the Ångström exponent (α) was 0.73 ± 0.27. Aerosol optical properties revealed significant seasonal characteristics. Frequent sandstorms in MAM (March–April–May) resulted in the seasonal maximum AOD, 0.41 ± 0.04, and a relatively smaller α value, 0.44 ± 0.04. The tourism seasons, JJA (June–July–August) and SON (September–October–November) coincide with serious emissions of small anthropogenic aerosols. While in DJF (December–January–February), the composition of the atmosphere was a mixture of dust particles and polluted aerosols released by domestic heating; the average AOD and α were 0.29 ± 0.02 and 0.66 ± 0.17, respectively. Different air masses exhibited different degrees of influence on the aerosol concentration over Dunhuang in different seasons. During MAM, ranges of AOD (0.11–1.18) and α (0.06–0.82) were the largest under the dust influence of northwest-short-distance air mass in the four trajectories. Urban aerosols transported by northwest-short-distance air mass accounted for a very large proportion in JJA and the mixed aerosols observed in SON were mainly conveyed by air masses from the west. In DJF, the similar ranges of AOD and α under the three air mass demonstrated the analogous diffusion effects on regional pollutants over Dunhuang.

Key words: Dunhuang, AOD, Ångström exponent, dust aerosol, anthropogenic aerosols

Citation: Ma, Y. J., and Coauthors, 2017: Optical properties and source analysis of aerosols over a desert area in Dunhuang, Northwest China. *Adv. Atmos. Sci.*, **34**(8), 1017–1026, doi: 10.1007/s00376-016-6224-6.

1. Introduction

Aerosols are mixtures of suspended liquid and solid particles released by natural sources and anthropogenic activities, with diameters ranging from 10^{-3} to 10^{2} μm. Due to the effect of topography, surface properties, anthropogenic activities, and meteorological conditions, aerosols exhibit strong temporal and spatial variability (Kim et al., 2007; Mahowald et al., 2011; Power et al., 2006). Aerosols can change the earth–atmosphere radiance balance and energy budget, as well as affect the climate directly by absorbing and scattering sunlight. Additionally, hydrophilic aerosols can serve as cloud condensation nuclei or ice nuclei, thus having the potential to alter cloud properties and indirectly impact the climate (Dubovik et al., 2000; Che et al., 2009). As a result of their direct and indirect climatic effects, atmospheric aerosols have become a hot topic for the international scientific research community (IPCC, 2013). To obtain a comprehensive picture of aerosol optical properties in the long term, an extensive number of observational stations situated in various background ecosystems are required (Alados-Arboledas et al., 2008). Consequently, many countries and organizations have established aerosol observation networks, such as AERONET (USA) (Holben et al., 1998), AEROCAN (Canada) (Bokoye et al., 2001), PHOTONS (France) (Goloub et al., 2008), and CARSNET (China) (Che et al., 2015a), equipped with CIMEL sun-photometers;

* Corresponding author: Jinyuan XIN
Email: xjy@mail.iap.ac.cn

SKYNET (Japan) (Uchiyama et al., 2005), equipped with sky-radiometers; and GALION [WMO-GAW(Global Atmosphere Watch)] (Bösenberg et al., 2008), equipped with an aerosol lidar system. The Institute of Atmospheric Physics, Chinese Academy of Sciences, and the University of Maryland jointly developed China's first and largest set of ground-based aerosol observation platforms; namely, the Chinese Sun Hazemeter Network (CSHNET), launched in July 2004 (Xin et al., 2007; Wang et al., 2007). CSHNET had 23 stations in the initial stage, with LED hazemeters employed for observing regional aerosol optical properties. During 2011–12, substantial progress was made towards further improving the network under the support of CARE-China (Campaign on Atmospheric Aerosol Research Network of China) (Xin et al., 2015). Presently, there are 36 operating stations, and the Microtops-II sun-photometer is used to host the whole network.

Dunhuang is located in the westernmost region of the Hexi Corridor, and serves as the geographical meeting-point of three provinces (Gansu, Qinghai, and Xinjiang). Dunhuang has an area of 3.12×10^4 km^2, of which almost 95.5% is covered by the Gobi desert (Liu et al., 2005). Acting as a typical arid-desert background region, Dunhuang has been a research hot-spot for scientists both at home and abroad (Trochkine et al., 2003, 2012; Xia et al., 2004; Shen et al., 2006; Yan, 2007; Gao et al., 2013). Xia et al. (2004) conducted a regional aerosol observation experiment in Dunhuang during 1999–2000, and found an annual average AOD loading of 0.24 and Ångström exponent (α) of 0.21. They clearly noted that dust aerosols were individually controlling the atmospheric components all year round. To further analyze the effect of dust transported from Northwest China to Japan, using a seasonal sampling dataset from Dunhuang provided by the ACE-Asia project, Trochkine et al. (2012) discovered similar dust constituents in component analysis of different seasons, and pointed out that they were identical to the material suspended inside the troposphere over Japan. Liu and Yue (2007) investigated AOD variation under different weather conditions for Dunhuang in spring. They noted that AOD values were less than 0.3 on clear-sky days. With floating dust, AOD was two to three times higher. Values that were two to three times larger than during weather conditions that offloaded dust were also apparent during sandstorms. Gao et al. (2013) explored the aerosol optical properties of northern China, and identified that coarse-mode dust dominated during 2004–07. In the past decade, with increasing population growth and the development of the tourism industry, the economic structure of Dunhuang has changed dramatically. Dunhuang statistical yearbook (Dunhuang Statistical Bureau, 2000–2012) showed that annual average tourist numbers increased almost fivefold during the 14 years from 1999 to 2012. High levels of immigration can raise the demand for urbanization, which in turn can lead to a greater abundance of anthropogenic aerosols, resulting in increasingly more complex aerosol pollution. Different aerosol types possess different scattering and absorption properties, with different signs and magnitudes of aerosol radiative forcing (Satheesh and Moorthy, 2005). For example, dust aerosols are hydrophobic coarse particles, absorbing short wavelength radiation, whereas fine-mode black carbon is a strongly hygroscopic aerosol (Lund and Berntsen, 2013). Relatively smaller sulfate aerosols can reflect solar light back to space and also exhibit strong hygroscopic behavior. The different climatic effects of aerosols seriously affect regional climate change (Ramanathan and Carmichael, 2008). As a consequence, an in-depth study on the aerosol optical properties and changes in aerosol components over the Dunhuang region is urgently required.

2. Methods and data

2.1. *Site description*

The Dunhuang Desert background station [(40°01′N, 94°04′E); altitude of 1140 m] of CARE-China is located in the yard of Dunhuang Meteorology Bureau (Fig. 1). Dunhuang is a typical desert basin, with the Qilian mountains to the south, Kumtag desert and Lop Nur to the west, Beisai mountain to the north, and Sanwei mountain to the east. Besides, the famous Taklimakan and Tengger deserts are also located in the west and east of Dunhuang region, respectively. Dunhuang has a warm-temperate arid climate, with four distinctive seasons. Annual mean temperature is 9.3°C. Annual mean precipitation is 38.7 mm, and the annual mean potential evaporation is 2476.4 mm (Liu et al., 2005).

2.2. *Instrumentation*

The spectral extinction method is an effective technique widely used to capture aerosol optical properties. It uses narrow-band sun-photometers to explore direct radiation, and then determines columnar AOD using the calculation module predefined in the instrument (Xin et al., 2006). Thirty six stations belonging to CARE-China are equipped with Microtops-II sun-photometers, a hand-held manually operated instrument, and provide observational AOD values. The physical properties and operational methods are introduced in detail in the instrument's instruction manual, which is publicly accessible (Solar Light Company, 2001). The Microtops-II sun-photometer receives solar irradiance in five channels (440 nm, 500 nm, 675 nm, 870 nm, and 936 nm), from which it automatically derives AOD through the AOD calculation module (details are described in section 2.3.1). Filters for the five channels all have a wavelength precision of ±1.5 nm, and a full width at half maximum band pass of 10 nm (Ichoku et al., 2002; Segla et al., 2011).

Due to the aging of optical filters and other influences, the accuracy of the Microtops-II sun-photometer can reduce over time. Hence, calibration is important to guarantee instrument precision. Langley calibration and transfer calibration are the two main methods normally used to calibrate the photometers. In August or September of each year, Langley calibration is performed in Lhasa. Then, the calibrated instrument is transferred to calibrate the other photometers (Xin et al., 2011, 2014).

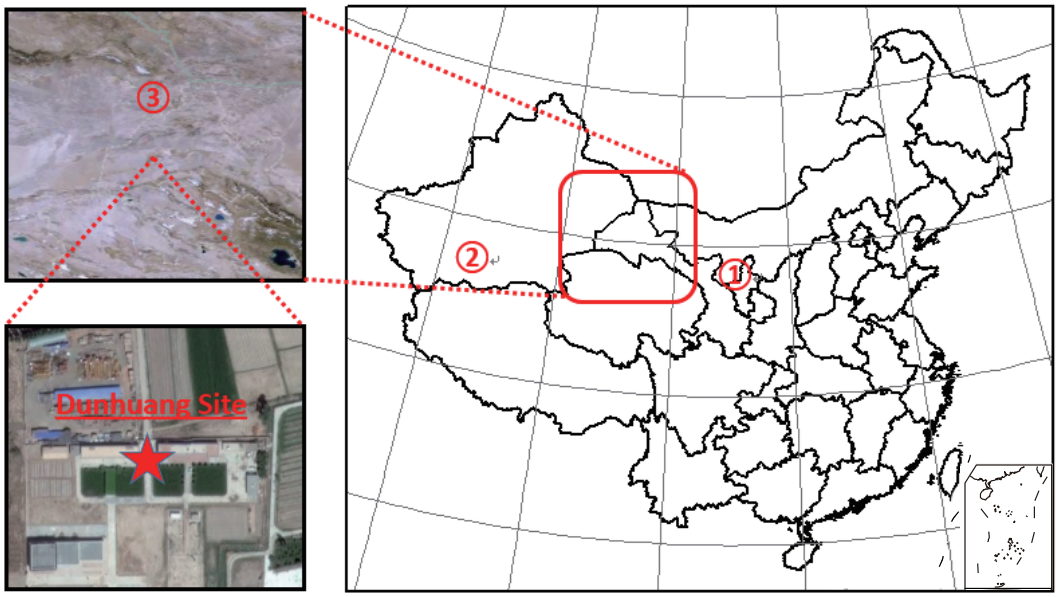

Fig. 1. Geographical location of Dunhuang station. ①: Tengger Desert; ②: Taklimakan Desert; ③: Kumtag Desert.

2.3. *Data processing*

2.3.1. *AOD calculation*

An AOD inversion algorithm based on the fundamental theory of the Beer–Lambert–Bouguer law was programed into the Microtops-II sun-photometer. The Beer–Lambert–Bouguer law is an atmospheric transmission and extinction model, as shown below (Ichoku et al., 2002):

$$V_\lambda = V_{\lambda,0} D^{-2} e^{-m\tau_{\mathrm{Tot},\lambda}} , \tag{1}$$

where, for each wavelength, V_λ is the output voltage signal observed by the Microtops-II sun-photometer; $V_{\lambda,0}$ is the extraterrestrial voltage signal; D is the sun–earth distance, in astronomical units, at the time of observation; m is optical air quality; and $\tau_{\mathrm{Tot},\lambda}$ is the total atmospheric columnar optical depth,

$$\tau_{\mathrm{Tot},\lambda} = \tau_{\mathrm{Ray},\lambda} + \tau_{\mathrm{aer},\lambda} + \tau_{\mathrm{O_3},\lambda} ,$$

in which $\tau_{\mathrm{Ray},\lambda}$ is the Rayleigh scattering optical depth, $\tau_{\mathrm{aer},\lambda}$ is the AOD, and $\tau_{\mathrm{O_3},\lambda}$ is the ozone optical depth.

The methods for calculating $\tau_{\mathrm{O_3},\lambda}$ and $\tau_{\mathrm{Ray},\lambda}$ are discussed in detail in Ichoku et al. (2002). Thus, $\tau_{\mathrm{aer},\lambda}$ is derived by

$$\tau_{\mathrm{aer},\lambda} = \frac{\ln(V_{\lambda,0}) - \ln(V_\lambda D^2)}{m} - \tau_{\mathrm{Ray},\lambda} - \tau_{\mathrm{O_3},\lambda} . \tag{2}$$

2.3.2. *Ångström exponent calculation*

According to the Junge distribution of aerosols, Ångström (1964) constructed a relational equation between wavelength and AOD:

$$\tau_{\mathrm{aer},\lambda} = \beta\lambda^{-\alpha} , \tag{3}$$

where, for each wavelength, $\tau_{\mathrm{aer},\lambda}$ is the AOD and β is the turbidity coefficient.

For any two wavelengths, the log-linear fitting formula is

$$\alpha = -\frac{\ln(\tau_{\mathrm{aer},\lambda_1}) - \ln(\tau_{\mathrm{aer},\lambda_2})}{\ln(\lambda_1) - \ln(\lambda_2)} \tag{4}$$

The α is an indicator of particle size, and the range is 0–2 (Peppler et al., 2000). When α approaches 0, it indicates that coarse-mode dust is dominant; as it approaches 2, it indicates that fine-mode smoke is dominant. A number of studies have compiled α ranges: urban-industrial aerosols are in the range of $1.1 < \alpha < 2.4$; black carbon aerosols are in the range of $1.2 < \alpha < 2.3$; and dust aerosols are in the range of $-1.0 < \alpha < 0.5$ (Tanré et al., 2001; Dubovik et al., 2002).

2.4. *Data*

This study employed observational AOD data from Dunhuang station of CARE-China and meteorological data from Dunhuang Meteorological Bureau for the whole year of 2012. The corresponding α data were calculated with AOD values in three channels (440 nm, 500 nm and 675 nm). The NOAA global reanalysis datasets, used for backward trajectory analysis, were downloaded from ftp://arlftp.arlhq.noaa.gov/pub/archives/reanalysis, which has a GBL (Global Latitude-Longitude Projection) format and a resolution of $2.5° \times 2.5°$.

3. Results

3.1. *Variation of aerosol loading and the Ångström exponent*

Figure 2 shows the annual and seasonal average values of AOD and α for the most recent decade [data for 1999 were obtained from Xia et al. (2004), observed by a sun/sky radiometer; data for 2004–07 were obtained from Gao et al. (2013), observed by the sky-radiometer of SKYNET). Annual averages for AOD and α were 0.32 ± 0.06 and $0.73 \pm$

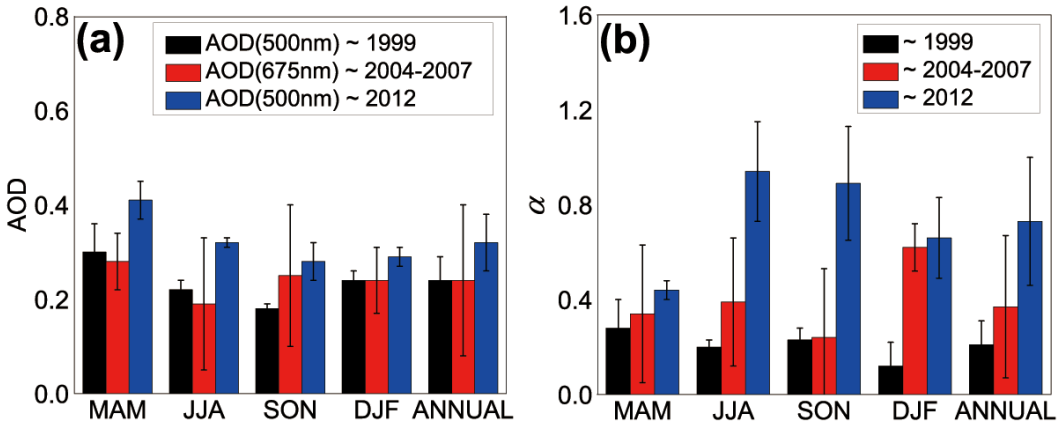

Fig. 2. Seasonal and annual average values and standard deviations of AOD and α.

0.27, respectively, in Dunhuang in 2012. The AOD value was lower than some typical values from urban aerosol studies in China. For example, the annual mean AOD at 440 nm was 0.42 in Kunming (Zhu et al., 2015), 0.59 at 500 nm in Shenyang (Che et al., 2015b), and 0.48 at 500 nm in Beijing (Xin et al., 2011). This comparison demonstrates that Dunhuang maintained a relatively clean environment. Both AOD and α values in 2012 were higher than those of 1999 (AOD_{500nm}, $\sim 0.24 \pm 0.05$; α, $\sim 0.21 \pm 0.10$) and 2004–07 (AOD_{675nm}, $\sim 0.24 \pm 0.16$; α, $\sim 0.37 \pm 0.30$), revealing an increasing trend both for AOD and α over the 14 years from 1999 to 2012. The increasing AOD demonstrated increasingly more serious pollution over this region, whereas the steep rise in α was generally related to the sufficiently higher emissions of fine particles. Che et al. (2015a) obtained the same upward AOD result by analyzing a long-term observational dataset (2002–13) provided by the CARSNET Dunhuang station, and they speculated that, although dust events were decreasing, floating dust particles may have been suspended in the air for a longer time. Dunhuang, as a famous resort, has attracted increasingly more tourists in recent years. The tourism population was 0.53 million in 1999, and it increased to approximately one million during the years of 2004–07, nearly double that of 1999. In 2012, it rose sharply to reach 3.1204 million, six times larger than that in 1999 (Dunhuang Statistical Bureau, 2000–2012). The considerable increase in tourists not only increased anthropogenic aerosol emissions, but also amplified vehicle usage, making it much more serious in terms of fine-particle pollution.

The order with respect to the seasonal mean AOD in Dunhuang in 2012 (Fig. 2a) was as follows: MAM (March–April–May; 0.41 ± 0.04) >JJA (June–July–August; 0.32 ± 0.01) >DJF (December–January–February; 0.29 ± 0.02) >SON (September–October–November; 0.28 ± 0.04). By contrast, the highest seasonal AOD values have been found to exist in summer over Shanghai (He et al., 2012) and Wuhan (Wang et al., 2014). This difference mainly comes from the different environmental backgrounds and origins of aerosols. The maximum α of 0.94 ± 0.21 among the four seasons occurred in JJA, and the other three values were 0.89 ± 0.24 (SON), 0.66 ± 0.17 (DJF) and 0.44 ± 0.04 (MAM). In MAM, intense atmospheric activities provide a mechanism for the injection of substantial amounts of dust material into the lower and middle troposphere (Yumimoto et al., 2009), resulting in the maximum AOD and the corresponding minimum α. During the tourism seasons (JJA and SON), increased human activities led to high concentrations of fine particles, and fine-mode pollution became significantly more obvious with the increase in the number of tourists (Fig. 2). DJF is the season when domestic heating is used most, in which the atmospheric composition is dominated by fine-mode black carbon aerosols, sulfate aerosols and occasional coarse-mode dust.

Figure 3 presents the monthly average values of AOD at 500 nm and the α. Figure 3a shows that the monthly average AOD values varied slightly. The maximum (0.44 ± 0.22) occurred in March, followed by 0.42 ± 0.28 in May and 0.35 ± 0.17 in April, suggesting that Dunhuang was seriously affected by frequent dust events in MAM. Of the remaining months, the AOD value of 0.33 ± 0.15 in November was the largest. This was possibly related to the frequent occurrence of dust weather (over the 10-day records of the whole of November). The monthly variation of α exhibited severe fluctuation in 2012 (Fig. 3b), demonstrating the dominant mode was different in different periods. The α values of February–May were relatively small, i.e., lower than 0.5, which was associated with the frequent occurrence of sandstorms in MAM. The peak of α was in June–October, with an annual maximum value of 1.16 ± 0.21 occurring in August. These fine-mode particles were mainly due to the intense radiation during summer, which provided ample energy for chemical reactions, and thereby generated large amounts of fine-mode secondary aerosol pollution. Additionally, increasing emissions of inorganic compounds (including sulfide, oxynitride, hydrocarbons etc.) and organic compounds (including alkane, olefin, aromatic hydrocarbons etc.) (Fanick et al., 2015; Kojima et al., 2016) were emitted during the peak tourism period of May–October. In November, the number of tourists declined and, due to the frequency of sand-dust, the α value (0.54 ± 0.24) was relatively lower. December and January were months when domestic heating was required, meaning sustained coal combustion and abundant

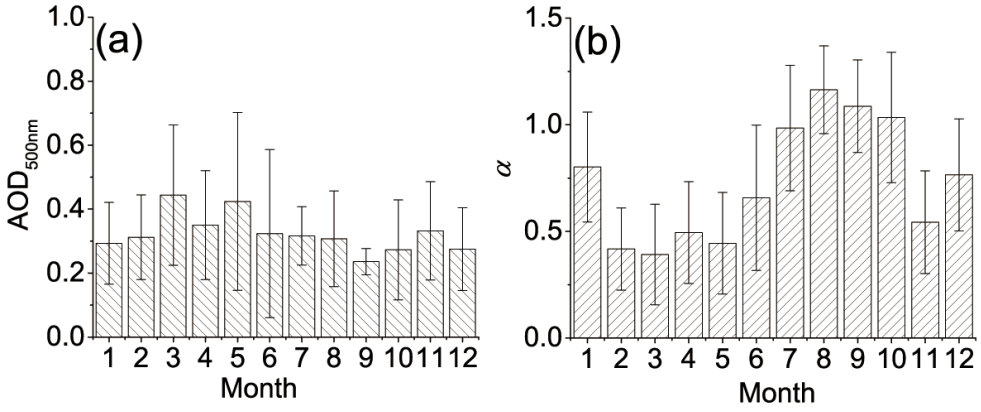

Fig. 3. Monthly average values and standard deviations of (a) AOD and (b) α.

fine-mode black carbon aerosols and sulfate aerosols were a feature. Thus, α exhibited much larger values.

3.2. *Frequency distribution of AOD and Ångström exponent*

The annual and seasonal frequency histograms of both AOD and α are shown in Fig. 4. The aim is to reveal how the distribution of aerosol optical properties changed with the seasons, which can help in identifying the major aerosol types (Pace et al., 2006; Salinas et al., 2009).

The annual frequency distributions of AOD and α exhibited a single peak. The maximum frequency of annual AOD (Fig. 4a) was observed in the 0.2–0.4 range and accounted for 54.98%. As for the seasonal AOD frequency distribution (inset figure in Fig. 4a), the peaks of the four seasons were commonly situated within the range 0.2–0.4. The frequency values of JJA, SON and DJF in each range all appeared to be similar. However, compared with the former three seasons, although the MAM frequency values in the first two ranges (<0.2 and 0.2–0.4) were both smaller, the frequency value of 31.75% in the 0.4–0.6 range was much larger, which is additional evidence for serious MAM pollution. The maximum frequency value of 18.65% of annual α (Fig. 4b) was observed in the 0.4–0.6 range, and the next two ranges, 0.6–0.8 and 0.8–1.0, were 17.86% and 17.46%, respectively. This illustrates the complexity of aerosol types. Extreme differences existed for the seasonal α frequency distribution (inset figure in Fig. 4b). A maximum frequency of 28.57% for MAM occurred in the 0.2–0.4 range; a maximum frequency of 24.62% for DJF occurred in the 0.6–0.8 range. The fitting curves of JJA and SON were similar, with the maximum of 22.64% in JJA situated at 1.0–1.2, and the maximum of 27.14% in SON at 0.8–1.0. Xia et al. (2004) found the maximum α frequencies for the four seasons all appeared within 0.0–0.2 over Dunhuang in 1999; that is, dust aerosols were the dominant mode throughout the whole year. Comparison revealed that, in the most recent decade, dust aerosols still played a principal role in MAM but, due to the decrease in dust weather, α increased slightly. Because of the increasing contribution of human activities, the main mode of control for the other three seasons changed. As tourist numbers increased rapidly, the proportion of anthropogenic aerosols presented an increasing trend. Urban and urban-dust aerosols were the main components in JJA and SON, respectively. During DJF, the effect of coal combustion gradually became obvious, so occasional dust, black carbon and sulfate aerosols coexisted.

3.3. *Backward trajectory clusters*

To analyze air mass origins for the Dunhuang region in the year of 2012, we employed the TrajStat (Trajectory Statistics) model (http://ready.arl.noaa.gov/HYSPLIT.php) for seasonal backward trajectory clustering. The TrajStat model is software developed by NOAA HYSPLIT users (Wang et al., 2009), using the same trajectory calculation module as HYSPLIT. The input meteorological data were from the NOAA global reanalysis dataset. In the simulation, the starting height was set to 1000 m and the endpoint was Dunhuang Meteorology Bureau. The backward time was 72 hours. The clustering results are displayed in Fig. 5.

The seasonal cluster results (Fig. 5) showed that MAM air masses individually consisted of four types, whereas the other three seasons were clustered into three common types. Northwest–short-distance air masses occurred throughout the four seasons, and were dominant in MAM, JJA, and SON. However, in DJF, west–long-distance air masses were most common. Specific details for the seasonal trajectory clusters are as follows:

In MAM,

(1) Type-1: Northwest–short-distance air mass. This air mass came from the northwest of Turpan Depression and accounted for 58.15% of the total air masses for this season.

(2) Type-2: West–long-distance air mass. This air mass came from west of Taklimakan Desert and accounted for 25.27% of the total air masses for this season.

(3) Type-3: Northwest–long-distance air mass. This air mass came from west of Novosibirsk and accounted for 10.87% of the total air masses for this season.

(4) Type-4: Northeast–long-distance air mass. This air mass came from central Outer Mongolia and accounted for 5.71% of the total air masses for this season.

In JJA,

(1) Type-1: Northwest–short-distance air mass. This air

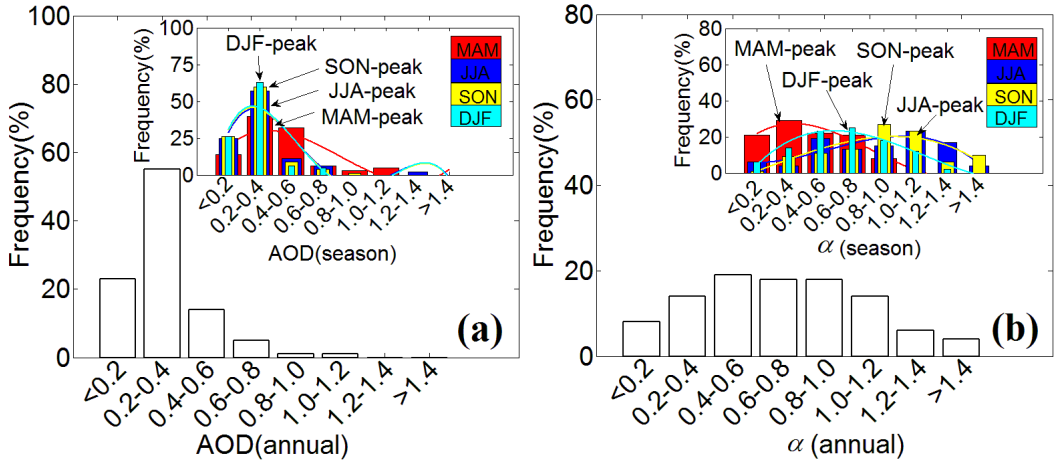

Fig. 4. Annual and seasonal frequency distribution of (a) AOD and (b) α. Solid lines in the two inset figures represent the fitting curves that best fit the data distribution.

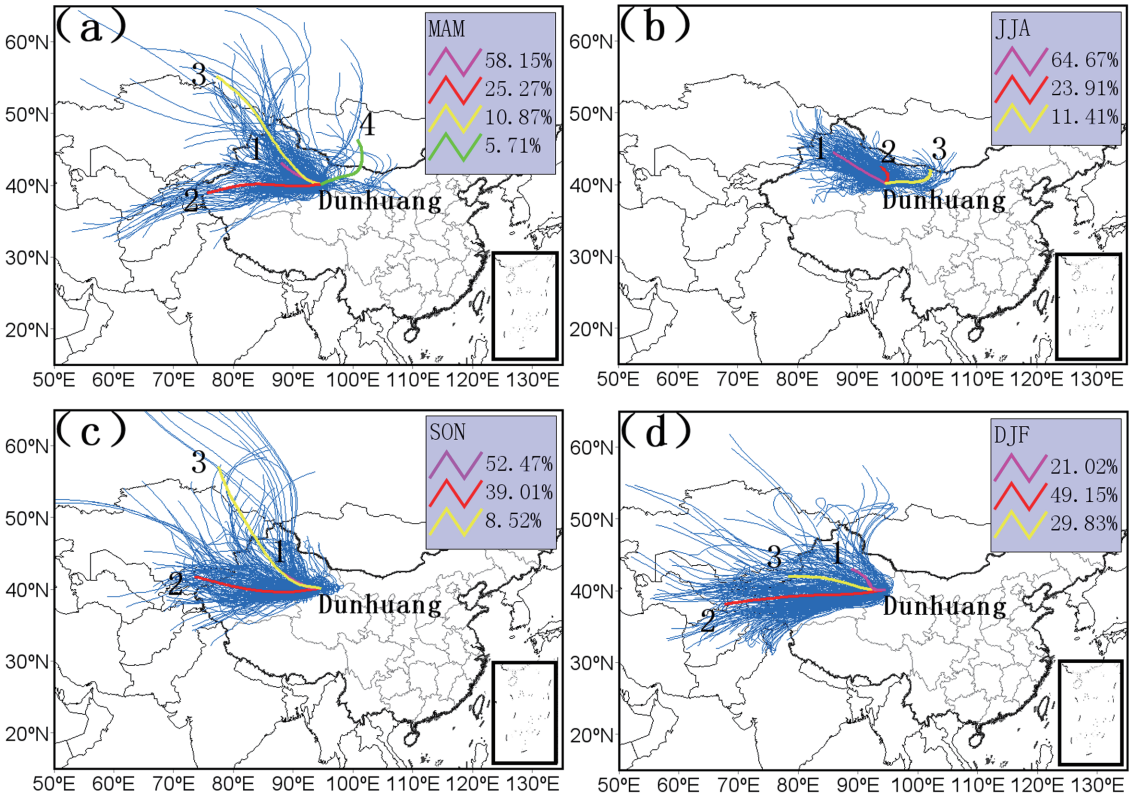

Fig. 5. Seasonal backward-trajectory clustering of the Dunhuang station: (a) MAM; (b) JJA; (c) SON; (d) DJF. Blue lines represent the specific backward-trajectory of each day.

mass came from the central Gurbantünggüt Desert and accounted for 64.47% of the total air masses for this season.

(2) Type-2: North–short-distance air mass. This air mass came from east of Turpan Depression and accounted for 23.91% of the total air masses for this season.

(3) Type-3: Northeast–short-distance air mass. This air mass came from north of Badain-Jaran Desert and accounted for 11.42% of the total air masses for this season.

In SON,

(1) Type-1: Northwest–short-distance air mass. This air mass came from northwest of Turpan Depression and accounted for 52.47% of the total air masses for this season.

(2) Type-2: West–long-distance air mass. This air mass came from central Kyrgyzstan and accounted for 39.01% of the total air masses for this season.

(3) Type-3: Northwest–long-distance air mass. This air mass came from west of Novosibirsk and accounted for 8.52% of the total air masses for this season.

In DJF,

(1) Type-1: Northwest–short-distance air mass. This air mass came from northwest of Turpan Depression and accounted for 21.02% of the total air masses for this season.

(2) Type-2: West–long-distance air mass. This air mass came from the southeast of Uzbekistan and accounted for 49.15% of the total air masses for this season.

(3) Type-3: Northwest-by-west–short-distance air mass. This air mass came from the east of Kyrgyzstan and accounted for 29.83% of the total air masses for this season.

In MAM, northwest air masses occupied the largest proportion, i.e., 69.02% (Type-1: northwest–short-distance air masses accounted for 58.15%; Type-3: northwest–long-distance air masses accounted for 10.87%). Under the influence of northwest air masses, the α values were 0.42 ± 0.22 (Type-1) and 0.33 ± 0.16 (Type-3), smaller than those of 0.72 ± 0.21 (Type-4) and 0.61 ± 0.27 (Type-2) and thus demonstrating that coarse-mode dust aerosols carried by northwest air masses when blowing through the Kumtag Desert and Lop Nur seriously polluted the Dunhuang area and were responsible for the occurrence of the highest AOD values of 0.44 ± 0.26 (Type-1) and 0.42 ± 0.15 (Type-3). Northwest air masses still played a leading role in JJA, with a frequency of 64.67%, but because of the comparatively lower wind speed of 1.73 ± 0.48 m s^{-1}, the dust could not be uplifted and AOD was low. The Type-2 air masses originating from the eastern Turpan Depression were accompanied by the highest wind speeds of 2.52 ± 1.14 m s^{-1}. These air masses picked up dust and continental aerosols when passing through the Gobi Desert region and eventually affected the Dunhuang area, leading to the highest AOD of 0.50 ± 0.36. In SON, dust weather was mainly concentrated in November. There were dust records of over 10 days in November; nevertheless, seven of these records were controlled by Type-1 (northwest–short-distance air masses), indicating that dust aerosols transferred by northwest air masses affected the Dunhuang region as well. Observed AOD values under the three types of air masses in DJF were similar, with differences of only 0.02, and the α values showed differences of 0.13. Thus, it is obvious that there was no significant diversity for the three types. Pollution mainly came from the diffusion of regional black carbon and sulfate aerosols generated by coal combustion.

From the above, similar air mass types appeared in MAM, SON and DJF alike, except for the northeast air masses (Type-4) of MAM. The highest AOD values were commonly commanded by the northwest–short-distance air masses (Type-1) for the three seasons mentioned above. Taking Type-1 air masses of the four seasons into consideration, it is distinctly evident that wind speed was the major meteorological factor. The α decreased with increasing wind speed (Table 1). The west–long-distance air masses of the three seasons (MAM, SON, and DJF) transported considerable amounts of dust aerosols from the Taklimakan Desert. The Taklimakan Desert is situated in the central Tarim basin. To the north of the Tarim basin are the Tianshan Mountains, and to the south and east are the Karakoram Range, Kunlun Mountains and Altun Mountains, with an average ridge line height of 5000–6000 m. These mountains had a striking effect on the blocking and settling of aerosol particles, so that west air masses did not cause an increase in AOD. The northeast air masses only influenced the region in MAM and JJA. They polluted the Dunhuang region through traversing the Hexi Corridor.

3.4. *Analysis of aerosol source*

To analyze the aerosol source of Dunhuang region, we employed the methodology of a classification frame-diagram to sort the aerosols under different air mass types of different seasons (Kaskaoutis et al., 2007). The classification frame-diagram is shown as Fig. 6. Each category subsection of the frame-diagram is defined by threshold values of AOD and α for the corresponding aerosol type. The classification basis of the threshold is shown in Table 2 (Tanré et al., 2001; Dubovik et al., 2002; Kaskaoutis et al., 2007).

Figure 7 presents seasonal scatterplots for AOD versus α against the classification frame-diagram in different air masses. In MAM, dust aerosols were the dominant components, freely affected from biomass burning/urban aerosol types (Fig. 7a). Dust aerosols mainly occurred under the control of Type-1 and Type-3 air masses. In the Type-1 air

Table 1. Attributes of different air masses and the corresponding average AOD, α, and wind speed (WS) values in different seasons.

	Time	Origin	Direction/distance	Percent	AOD	α	WS (m s^{-1})
Type-1	MAM	Northwest of Turpan Depression	Northwest/short	58.15%	0.44 ± 0.26	0.42 ± 0.22	2.21 ± 1.02
	JJA	Central Gurbantünggüt Desert	Northwest/short	64.67%	0.27 ± 0.12	0.97 ± 0.34	1.73 ± 0.48
	SON	Northwest of Turpan Depression	Northwest/short	52.47%	0.33 ± 0.18	0.70 ± 0.29	1.76 ± 0.72
	DJF	Northwest of Turpan Depression	Northwest/short	21.02%	0.30 ± 0.14	0.60 ± 0.25	2.14 ± 0.84
Type-2	MAM	West of Taklimakan Desert	West/long	25.27%	0.27 ± 0.13	0.61 ± 0.27	2.76 ± 0.85
	JJA	East of Turpan Depression	North/Short	23.91%	0.50 ± 0.36	0.71 ± 0.40	2.52 ± 1.14
	SON	Central Kyrgyzstan	West/long	39.01%	0.24 ± 0.08	1.10 ± 0.26	1.83 ± 0.71
	DJF	Southeast of Uzbekistan	West/long	49.15%	0.28 ± 0.17	0.73 ± 0.32	2.35 ± 0.98
Type-3	MAM	West of Novosibirsk	Northwest/long	10.87%	0.42 ± 0.15	0.33 ± 0.16	2.82 ± 0.81
	JJA	North of Badain-Jaran Desert	Northeast/short	11.42%	0.34 ± 0.13	0.63 ± 0.25	2.49 ± 0.61
	SON	West of Novosibirsk	Northwest/long	8.52%	0.24 ± 0.09	0.85 ± 0.46	2.71 ± 0.92
	DJF	East of Kyrgyzstan	Northwest-by-west/short	29.83%	0.28 ± 0.12	0.70 ± 0.33	2.44 ± 1.08
Type-4	MAM	Central Outer Mongolia	Northeast/long	5.71%	0.32 ± 0.26	0.72 ± 0.21	3.93 ± 0.94
	JJA	—	—	—	—	—	—
	SON	—	—	—	—	—	—
	DJF	—	—	—	—	—	—

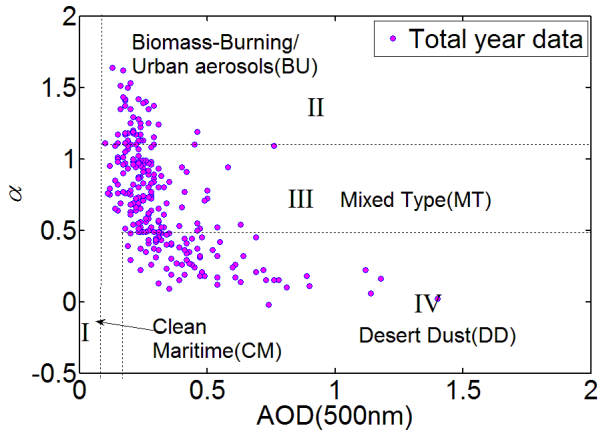

Fig. 6. A classification frame-display diagram for the total data of 2012 at Dunhuang. Each subsection indicates one type of aerosol: I: Clean maritime (CM); II: Biomass-burning/urban aerosols (BU); III: Mixed type (MT); IV: Desert dust (DD).

Table 2. Threshold values of AOD and α under the control of different aerosol types.

	AOD	α
I: Clean maritime	0–0.07	—
II: Biomass burning/urban aerosol	0.07–2	1.1–2
III: Mixed type	0.07–2	0.5-1.1
	0.07–0.2	−0.5 – 0.5
IV: Desert dust	0.2–2	−0.5 – 0.5

mass, the range of AOD was 0.11–1.18, and α was 0.06–0.82. Both were larger than the AOD range of 0.21–0.76 and the α range of 0.13–0.69 observed for Type-3, indicating that the Type-1 air masses played a much more conspicuous role in the Dunhuang region. The impact of dust weather was concealed by the prominent human activities during JJA. With the gradual increase of anthropogenic fine particles and secondary aerosols, the preferential urban aerosols became dominant (Fig. 7b). Urban aerosols mainly existed in the northwest–short-distance air masses (Type-1), in which the AOD range was 0.10–0.46 which was probably related to the exhaust fumes emitted by the large number of tour buses traveling between Dunhuang city and the famous northwest scenic sites (Ghost city, Yumen pass etc). The three types of SON all delivered dust aerosols (Fig. 7c), among which the northwest–short-distance air masses (Type-1) were the most dominant component. The maximum value of the daily average AOD was 0.89 under the influence of dust aerosols carried by Type-1, leading to severe pollution. In the Type-2 air masses, the AOD range was 0.16–0.32, and α was 0.68–1.53 (except for a rare continuous dust event that occurred on 4 November), indicating complex components containing both urban and dust aerosols. This phenomenon was also possibly related to the high number of motor vehicles traveling back and forth between Dunhuang city and the surrounding tourism areas. A mixture of black carbon, sulfate and dust aerosols coexisted during DJF (Fig. 7d). Ranges of AOD were 0.15–0.78, 0.15–0.69 and 0.17–0.54, respectively, un-

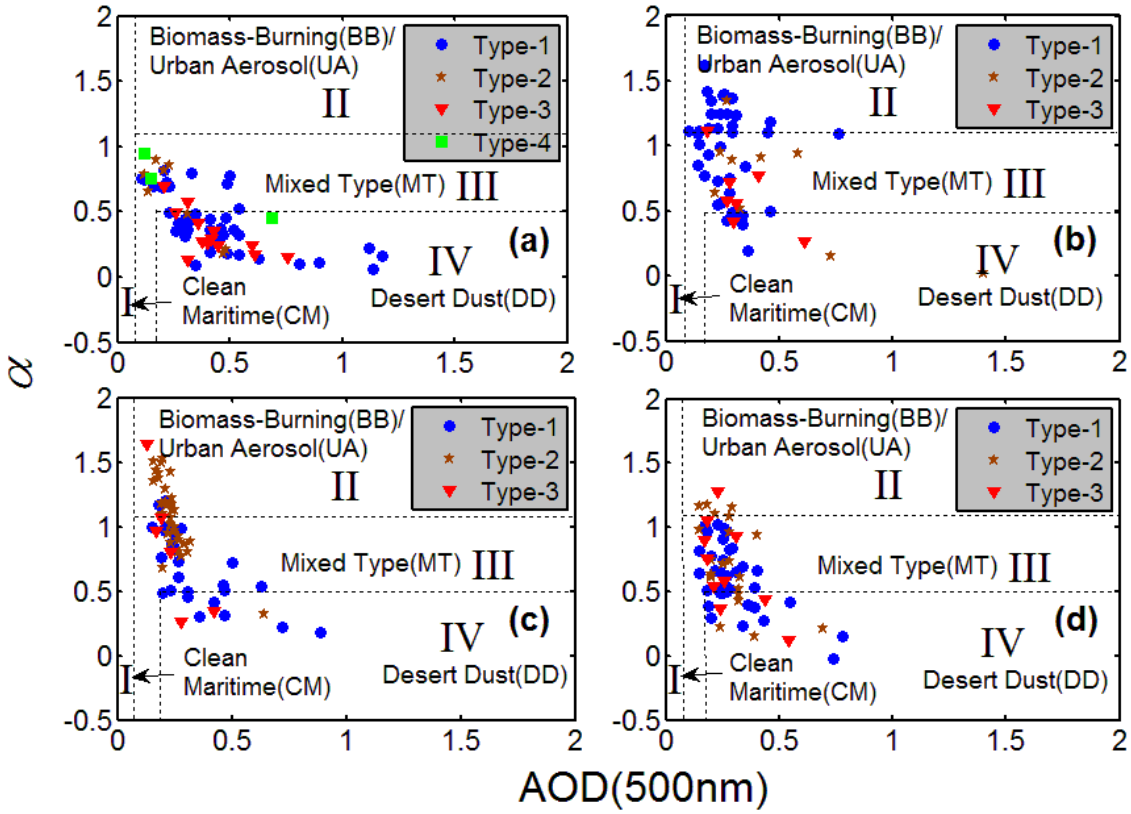

Fig. 7. Seasonal scatterplots for AOD versus α controlled by different air masses against the classification frame-display background: (a) MAM; (b) JJA; (c) SON; (d) DJF.

der the control of the Type-1, 2 and 3 air masses, and the corresponding α ranges were -0.02–1.02, 0.15–1.18 and 0.02–1.28, respectively, which suggested the effects of the three types on Dunhuang were similar. Regional coal combustion was the most important source of black carbon and sulfate aerosols, and the different air masses all exerted an effect on the spread of air pollution.

4. Conclusions

Through analyzing the aerosol observational datasets for 2012 obtained from Dunhuang station of CARE-China and comparing with previous aerosol observations in 1999 and 2004–07, we conclude that, due to the contribution of human activities, AOD rose in the most recent decade over the Dunhuang area. The α exhibited a similar increasing trend, and the main mode of control became a mixture of coarse and fine-mode particles from the previous single dust aerosol type. Significant seasonal characteristics were observed for the aerosol optical properties. The maximum AOD occurred in MAM, while the remaining three seasons were similar. Frequent dust weather events made dust aerosols the dominant component during MAM. The peak tourism season occurred in JJA and SON, and due to the significant human activities, fine urban aerosols were the main mode of control in JJA. For SON, the dust influences combined, and urban-dust aerosols occupied the maximum proportion. Numerous fine black carbon and sulfate aerosols were emitted by coal combustion in DJF, mixed with relatively frequent dust aerosols, resulting in the mixture type taking the principal position. Air mass types were similar in MAM, SON and DJF (except for Type-4 in MAM). In addition, Dunhuang was seriously affected by dust aerosols transported by high frequency Type-1 air masses of the three seasons, leading to the highest AOD values. Urban aerosols accounted for a considerable proportion in Type-1 (JJA) and Type-2 (SON). Regional coal combustion produced a large amount of fine pollution aerosols during DJF, and the three types of air masses exhibited similar diffusion behavior for the regional pollutants.

Acknowledgements. This study was partially supported by the National Natural Science Foundation of China (Grant Nos. 41375036 and 41222033), the National Basic Research Program of China (Grant No. 2016YFC0202001, 973 Program 2014CB441200) and the CAS Strategic Priority Research Program (Grant No. XDB05020103).

REFERENCES

Alados-Arboledas, L., and Coauthors, 2008: Aerosol columnar properties retrieved from CIMEL radiometers during VELETA 2002. *Atmos. Environ.*, **42**, 2654–2667.

Ångström, A., 1964: The parameters of atmospheric turbidity. *Tellus*, **16**, 64–75.

Bösenberg, J., and Coauthors, 2008: Plan for the Implementation of the GAW Aerosol Lidar Observation Network GALION. WMO TD No. 1443, 27–29 March 2007, Hamburg, Germany.

Bokoye, A. I., A. Royer, N. T. O'Neill, G. Fedosejevs, P. M. Teillet, and L. J. B. McArthur, 2001: Characterization of atmospheric aerosols across Canada from a ground-based Sunphotometer network: AEROCAN. *Atmos.-Ocean*, **39**, 429–456.

Che, H. Z., Z. F. Yang, X. Y. Zhang, C. Z. Zhu, Q. L. Mac, H. G. Zhou, and P. Wang, 2009: Study on the aerosol optical properties and their relationship with aerosol chemical compositions over three regional background stations in China. *Atmos. Environ.*, **43**, 1093–1099.

Che, H. Z., and Coauthors, 2015a: Ground-based aerosol climatology of China: Aerosol optical depths from the china aerosol remote sensing network (CARSNET) 2002–2013. *Atmos. Chem. Phys.*, **15**, 7619–7652.

Che, H. Z., and Coauthors, 2015b: Analyses of aerosol optical properties and direct radiative forcing over urban and industrial regions in Northeast China. *Meteor. Atmos. Phys.*, **127**, 345–354.

Dubovik, O., A. Smirnov, B. N. Holben, M. D. King, Y. J. Kaufman, and T. F. Eck, 2000: Accuracy assessments of aerosol optical properties retrieved from Aerosol Robotic Network (AERONET) Sun and sky radiance measurements. *J. Geophys. Res.*, **105**(D8), 9791–9806.

Dubovik, O., and Coauthors, 2002: Variability of absorption and optical properties of key aerosol types observed in worldwide locations. *J. Atmos. Sci.*, **59**, 590–608.

Dunhuang Statistical Bureau, 2000–2012: *Dunhuang Statistical Yearbook*.

Fanick, E. R., S. Kroll, and S. Simescu, 2015: Sampling System Investigation for the Determination of Semi-Volatile Organic Compounds (SVOC) Emissions from Engine Exhaust. SAE Technical Paper 2015-01-1062.

Gao, Z. M., J. R. Bi, and J. P. Huang, 2013: Analysis on aerosol optical property over Northern China from AERONET and SKYNET observations. *Plateau Meteorology*, **32**, 1293–1307. (in Chinese)

Goloub, P., and Coauthors, 2008: PHOTONS/AERONET sunphotometer network overview: Description, activities, results. *Proc. SPIE 6936, Fourteenth International Symp. on Atmospheric and Ocean Optics/Atmospheric Physics*, doi: 10.1117/12.783171.

He, Q. S., C. C. Li, F. H. Geng, H. Q. Yang, P. R. Li, T. T. Li, D. W. Li, and Z. Pei, 2012: Aerosol optical properties retrieved from Sun photometer measurements over Shanghai, China. *J. Geophys. Res.*, **117**(D16), D16204, doi: 10.1029/2011JD017220.

Holben, B. N., and Coauthors, 1998: AERONET-A federated instrument network and data archive for aerosol characterization. *Remote Sens. Environ.*, **66**, 1–16.

Ichoku, C., and Coauthors, 2002: Analysis of the performance characteristics of the five-channel Microtops II sun photometer for measuring aerosol optical thickness and precipitable water vapor. *J. Geophys. Res.*, **107**(D13), AAC 5-1–AAC 5-17.

IPCC, 2013: *Climate Change 2013: The Physical Science Basis. Contribution of Working Group I to the Fifth Assessment Report of the Intergovernmental Panel on Climate Change*, Stocker et al., Eds., Cambridge University Press, Cambridge, United Kingdom and New York, NY, USA, 1535 pp.

Kaskaoutis, D. G., H. D. Kambezidis, N. Hatzianastassiou, P. G. Kosmopoulos, and K. V. S. Badarinath, 2007: Aerosol climatology: On the discrimination of aerosol types over four AERONET sites. *Atmos. Chem. Phys.*, **7**, 6357–6411.

Kim, S. W., S. C. Yoon, J. Kim, and S. Y. Kim, 2007: Seasonal

and monthly variations of columnar aerosol optical properties over East Asia determined from multi-year MODIS, LIDAR, and AERONET sun/sky radiometer measurements. *Atmos. Environ.*, **41**, 1634–1651.

Kojima, R., N. Fukui, and H. Watanabe, 2016: Titanium oxide liquid dispersion, titanium oxide liquid coating, and photo catalyst coating film. European Patent Application EP2974793, issued 2014.

Liu, X. Y., and P. Yue, 2007: Inversion of the optical depth of aerosol over the Dunhuang region in spring. *Arid Zone Research*, **24**, 790–795. (in Chinese)

Liu, L. C., Z. B. Shen, T. Wang, M. X. Zhou, Y. Sadayo, and K. Shinji, 2005: Observation study on mass concentration of dust aerosols in Dunhuang. *Plateau Meteorology*, **24**, 765–771. (in Chinese)

Lund, M. T., and T. Berntsen, 2013: Contributions of diesel vehicle emissions to Arctic black carbon in the OsloCTM2. AGU Fall Meeting Abstracts, American Geophysical Union, 9–13 December 2013, San Francisco, USA.

Mahowald, N., and Coauthors, 2011: Aerosol impacts on climate and biogeochemistry. *Annual Review of Environment and Resources*, **36**, 45–74.

Pace, G., A. di Sarra, D. Meloni, S. Piacentino, and P. Chamard, 2006: Aerosol optical properties at Lampedusa (Central Mediterranean). 1. Influence of transport and identification of different aerosol types. *Atmos. Chem. Phys.*, **6**, 697–713.

Peppler, R. A., and Coauthors, 2000: ARM southern great plains site observations of the smoke pall associated with the 1998 central American fires. *Bull. Amer. Meteor. Soc.*, **81**, 2563–2592.

Power, H. C., S. C. Sheridan, and J. C. Senkbeil, 2006: Synoptic climatological influences on the spatial and Temporal variability of aerosols over North America. *Int. J. Climatol.*, **26**, 723–741.

Ramanathan, V., and G. Carmichael, 2008: Global and regional climate changes due to black carbon. *Nature Geoscience*, **1**, 221–227.

Salinas, S. V., B. N. Chew, and S. C. Liew, 2009: Retrievals of aerosol optical depth and Ångström exponent from ground-based sun-photometer data of Singapore. *Applied Optics*, **48**, 1473–1484.

Satheesh, S. K., and K. K. Moorthy, 2005: Radiative effects of natural aerosols: A review. *Atmos. Environ.*, **39**, 2089–2110.

Segla, A., A. Aguirre, and V. Vladutescu, 2011: Determination of Aerosol Optical Depth Using a Micro Total Ozone Spectrometer II (MICROTOPS II) Sun-photometer.

Shen, Z., J. J. Cao, X. X. Li, T. Okuda, Y. Q. Wang, and X. Y. Zhang, 2006: Mass concentration and mineralogical characteristics of aerosol particles collected at Dunhuang during ACE-Asia. *Adv. Atmos. Sci.*, **23**, 291–298, doi: 10.1007/s00376-006-0291-z.

Solar Light Company, 2001: Microtops II User's Guide. Solar Light Company, USA.

Tanré, D., and Coauthors, 2001: Climatology of dust aerosol size distribution and optical properties derived from remotely sensed data in the solar spectrum. *J. Geophys. Res.*, **106**, 18 205–18 217.

Trochkine, D., and Coauthors, 2003: Comparison of the chemical composition of mineral particles collected in Dunhuang, China and those collected in the free troposphere over Japan: Possible chemical modification during long-range transport. *Water, Air and Soil Pollution: Focus*, **3**, 161–172.

Trochkine, D., and Coauthors, 2012: Mineral aerosol particles collected in Dunhuang, China, and their comparison with chemically modified particles collected over Japan. *J. Geophys. Res.*, **108**(D23), doi: 10.1029/2002JD003268.

Uchiyama, A., A. Yamazaki, H. Togawa, and J. Asano, 2005: Characteristics of Aeolian dust observed by sky-radiometer in the Intensive Observation Period 1 (IOP1). *J. Meteor. Soc. Japan*, **83A**, 291–305.

Wang, L. L., J. Y. Xin, Y. S. Wang, Z. Q. Li, P. C. Wang, G. R. Liu, and T. X. Wen, 2007: Validation of MODIS aerosol products by CSHNET over China. *Chinese Science Bulletin*, **52**, 1708–1718.

Wang, Y. Q., X. Y. Zhang, and R. R. Draxler, 2009: TrajStat: GIS-based software that uses various trajectory statistical analysis methods to identify potential sources from long-term air pollution measurement data. *Environmental Modeling and Software*, **24**, 938–939.

Wang, L. C., W. Gong, X. A. Xia, J. Zhu, J. Li, and Z. M. Zhu, 2014: Long-term observations of aerosol optical properties at Wuhan, an urban site in Central China. *Atmos. Environ.*, **101**, 94–102.

Xia, X. A., H. B. Chen, and P. Wang, 2004: Aerosol properties in a Chinese semiarid region. *Atmos. Environ.*, **38**, 4571–4581.

Xin, J. Y., Y. S. Wang, Z. Q. Li, P. C. Wang, S. G. Wang, T. X. Wen, and Y. Sun, 2006: Introduction and calibration of the Chinese sun hazemeter network. *Environmental Science*, **27**, 1697–1702. (in Chinese with English abstract)

Xin, J. Y., and Coauthors, 2007: Aerosol optical depth (AOD) and angstrom exponent of aerosols observed by the Chinese sun hazemeter network from August 2004 to September 2005. *J. Geophys. Res.*, **112**(D5), doi: 10.1029/2006JD007075.

Xin, J. Y., L. L. Wang, Y. S. Wang, Z. Q. Li, and P. C. Wang, 2011: Trends in aerosol optical properties over the Bohai Rim in Northeast China from 2004 to 2010. *Atmos. Environ.*, **45**, 6317–6325.

Xin, J. Y., Q. Zhang, C. S. Gong, Y. S. Wang, W. P. Du, and Y. F. Zhao, 2014: Aerosol direct radiative forcing over Shandong Peninsula in East Asia from 2004 to 2011. *Atmos. and Oceanic Sci. Lett.*, **7**, 74–79.

Xin, J. Y., and Coauthors, 2015: The campaign on atmospheric aerosol research network of China: CARE-China. *Bull. Amer. Meteor. Soc.*, **96**, 1137–1155.

Yan, H., 2007: Aerosol scattering properties in northern China. *Atmos. Environ.*, **41**, 6916–6922.

Yumimoto, K., K. Eguchi, I. Uno, T. Takemura, Z. Liu, A. Shimizu, and N. Sugimoto, 2009: An elevated large-scale dust veil from the Taklimakan Desert: Intercontinental transport and three-dimensional structure as captured by CALIPSO and regional and global models. *Atmos. Chem. Phys.*, **9**, 8545–8558.

Zhu, J., X. A. Xia, H. Z. Che, J. Wang, J. Zhang, and Y. Duan, 2015: Study of aerosol optical properties at Kunming in southwest China and long-range transport of biomass burning aerosols from North Burma. *Atmos. Res.*, **169**, 237–247.